Threshold field for a nematic liquid crystal confined between two coaxial cylinders

A. Corella-Madueño, A. Castellanos-Moreno, S. Gutiérrez-López, and R. A. Rosas
Departamento de Física, Universidad de Sonora, Apartado Postal 1626, Hermosillo, Sonora, Mexico

J. A. Reyes
Departamento de Física Química, Instituto de Física, Universidad Nacional Autónoma de México, México D.F., C.P. 04510, Mexico

(Received 8 January 2008; revised manuscript received 25 June 2008; published 1 August 2008)

We consider a nematic liquid crystal constrained by two coaxial cylinders under the action of low-frequency axial or radial electric fields. Assuming an initially hybrid configuration, we find the equilibrium texture of the nematic subjected to weak anchoring boundary conditions on both cylindrical surfaces. We analyze the distinct textures of the nematic as a function of the strength of the interaction of the nematic with the sidewalls, the radii ratio of the cylinders, and the applied electric field. Also, for each radii ratio and strength of the nematic-surface interaction, we determine the critical field for which a complete alignment of the nematic liquid crystal occurs.

DOI: 10.1103/PhysRevE.78.022701 PACS number(s): 61.30.Gd, 61.30.Hn, 61.30.Dk

I. INTRODUCTION

Equilibrium configurations of nematic liquid crystals (NLCs) in a cylindrical cavity have been studied for approximately 40 years. The first of these calculations have been done by assuming hard anchoring homeotropic boundary conditions [1–3], and more recently arbitrary anchoring homeotropic boundary conditions have been considered to study the competition between bulk elastic energies imposed by the confining volume and molecular anchoring energies [4–7], including the effects of an applied low-frequency electric field [8].

The most convenient geometry to study NLCs after a geometry of plane-parallel cells is the cylindrical geometry, from both a theoretical and experimental point of view. In this case, essentially all experimentally observed and theoretically possible configurations of the director field **n** in a cylindrical cavity admit either a complete or approximate analytic description [7]. The possible equilibrium configurations of a nematic liquid crystal in a cylindrical cavity depend primarily on how the director **n** is anchored to the lateral surface of the cylinder.

A liquid-crystal material in its equilibrium configuration can exhibit three types of bulk deformations that are historically known as splay, twist, and bend. Each type of deformation is associated with a specific elastic constant K_1, K_2, and K_3, respectively, which describe the energy associated with the related deformations. For the surface elastic term proportional to K_4 (saddle-splay surface elastic constant) different definitions have been used by various researchers. For example, the K_4 distortion can result from liquid-crystal molecules being anchored to a curved surface [9], inhomogeneous configurations in planar cells [10], or hybrid aligned cells with parallel anchoring [11]. Here we will use the Saupe's description [12].

Surface elastic terms are unimportant in bulk quantities of liquid crystals and typically ignored. But when liquid crystals are confined to small cavities, its effect is found to be significant, particularly when elastic energies imposed by the confining volume compete with molecular anchoring energies [5].

Halevi *et al.* [13] established the existence of a phase transition—from the escaped radial (ER) to the axial (AX) configuration—within a single NLC cylinder reaching for a critical value of an axial applied field $\mathbf{E}_0$. They also demonstrated that varying E_0 in NLC-infilled photonic crystals the photonic band gap can be fully tuned from open to closed. These results could lead to tunable optical wave guides, switches, limiters, and polarizers, to reconfigurable optical networks, and to electro-optic interconnectors in microelectronics. The elastic interaction of liquid crystals within cylindrical confinements is also useful to describe liquid-crystal photonic crystal fibers which are a new class of optical waveguides. In general, liquid crystals, infiltrated in photonic crystal fibers, allow an effective electrical control of such optical waveguides [14,15].

The purpose of this paper is to study the configuration of a NLC confined within two coaxial cylinders subjected to an axially or radially applied electric field to determine the threshold field for which the nematic is completely aligned. To this end we state the total free energy of the NLC, from which we obtain the equilibrium equations by assuming weak anchoring conditions on both internal and external cylindrical surfaces. Then, we solve numerically the equilibrium equations and find the threshold fields for the two selected directions, axial or radial field, parametrized by the cylinders radii ratio and the strength of the interaction of the NLC with the walls. In this way, we characterize the field values for which both axial structure (AX or total escape) or planar-radial structure (PR or smectic like) can occur.

II. THRESHOLD FIELD

Let us consider a nematic liquid crystal confined between two coaxial cylindrical surfaces whose internal and external radii are R_1 and R_2, respectively. The z axis coincides with the cylinder axis and the director is weakly anchored to the surfaces of the cylinders with preferential directions parallel and perpendicular to the internal and external cylinders, respectively.

We shall assume that under these arbitrary boundary conditions the initial nematic's orientation occurs in the plane r-z and that is only a function of r; that is, the director $\hat{\mathbf{n}}$ is given by $\hat{\mathbf{n}}=[\sin\theta(r),0,\cos\theta(r)]$, where θ is defined in Fig. 1.

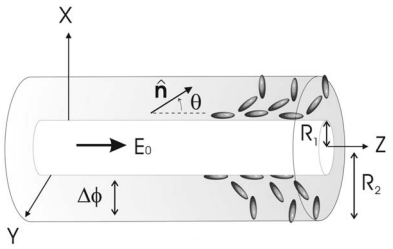

FIG. 1. Sketch of two coaxial cylindrical capillaries infiltrated by a nematic liquid crystal and subjected to a low-frequency electric field axially or radially applied.

The Frank's elastic free energy F_{elast} is given by

$$F_{elast} = \frac{1}{2}\int_V \{K_1(\nabla\cdot\hat{\mathbf{n}})^2 + K_2(\hat{\mathbf{n}}\cdot\nabla\times\hat{\mathbf{n}})^2 + K_3(\hat{\mathbf{n}}\times\nabla\times\hat{\mathbf{n}})^2 - K_4\nabla\cdot[\hat{\mathbf{n}}\times\nabla\times\hat{\mathbf{n}} + \hat{n}\nabla\cdot\hat{\mathbf{n}}]\}dv + \frac{1}{2}\int_{S_1} W_\theta \sin^2\phi_1\, ds_1 + \frac{1}{2}\int_{S_2} W_\theta \sin^2\phi_2\, ds_2, \quad (1)$$

where K_4 is the coefficient of a divergence term which can be transformed to a surface integral by using Gauss's theorem [12]. The two last terms provide the interaction between the NLC and the confining surfaces [16]. There ϕ_1 and ϕ_2 denote the angles between $\hat{\mathbf{n}}$ and the preferred direction of alignment at the surface and W_θ denotes the strength of the interaction in units of energy per area, which we will assume the same for both surfaces. For our system we have $\phi_1=\theta$ at $r=R_1$ and $\phi_2=\pi/2-\theta$ at $r=R_2$.

Then by expressing $\nabla\cdot\hat{\mathbf{n}}$ and $\nabla\times\hat{\mathbf{n}}$ in cylindrical coordinates we obtain the free energy $\mathcal{F}_{elast}$ per unit length:

$$\mathcal{F}_{elast} = \pi K_1\int_{R_1/R_2}^{1}\left[\left(\frac{d\theta}{dx}\right)^2(\cos^2\theta+\kappa\sin^2\theta)+\frac{\sin^2\theta}{x^2}\right]x\,dx + \pi K_1\left[\sigma_2\cos^2\theta(R_2)-\sigma_1\cos^2\theta(R_1)+\frac{R_1W_\theta}{K_1}\right], \quad (2)$$

where $\kappa=K_3/K_1$, $x=r/R_2$, and $\sigma_1=R_1W_\theta/K_1+K_4/K_1-1$ and $\sigma_2=R_2W_\theta/K_1+K_4/K_1-1$ are the dimensionless surface anchoring parameters.

A. Axial electric field

The contribution to the total free energy taking into account the interaction of NLC with an external electric field is expressed by the electric free energy F_{elect}. By taking $\mathbf{E}_0$ along the z axis, in SI units the F_{elect} is given by

$$F_{elect} = -\frac{1}{2}\int_V \epsilon_{zz}(r)E_0^2\,dv. \quad (3)$$

Now we express the element of the dielectric tensor $\epsilon_{zz}(r)$ in terms of the perpendicular and parallel dielectric permittivities of the NLC, $\epsilon_\perp$ and $\epsilon_\parallel$, respectively. At a point where the director forms an angle with the z axis, the dielectric tensor in the proper coordinate system of the NLC has an uniaxial form. This must be transformed into the "laboratory" coordinate system x,y,z, resulting in the following expression for the dielectric tensor elements: $\epsilon_{ij}=\epsilon_\perp\delta_{ij}+\epsilon_a n_i n_j$, where $\epsilon_a=\epsilon_\parallel-\epsilon_\perp$ is the dielectric anisotropy and the director defined above can be written as $\hat{\mathbf{n}}=\sin\theta(r)\mathbf{e}_r+\cos\theta(r)\mathbf{e}_z$, where $\mathbf{e}_r$ and $\mathbf{e}_z$ are the cylindrical unit vectors along the r and z directions, respectively. For infinite circular cylinders the symmetry implies that θ only depends on the radial distance r. Since $\hat{\mathbf{n}}$ is a position dependent vector, ϵ_{ij} shows explicitly that we have inhomogeneity, as well as anisotropy.

Using Eq. (3) and ϵ_{ij}, the electric energy per unit length, $\mathcal{F}_{elect}$, becomes

$$\mathcal{F}_{elect} = -\pi K_1 q_a\int_{R_1/R_2}^{1}\left(\frac{\epsilon_\perp^s}{\epsilon_a^s}+\cos^2\theta\right)x\,dx, \quad (4)$$

where ϵ_a^s is the low-frequency dielectric constant and q_a is an important dimensionless parameter defined as $q_a \equiv \epsilon_a^s E_0^2 R_2^2/K_1$, which represents the ratio of the electric and elastic energies; for $q_a \ll 1$, the influence of the applied field is weak, while for $q_a \gg 1$, the field essentially overcomes the elastic forces between the molecules.

Using Eqs. (2) and (4), the total free energy per unit length, $\mathcal{F}=\mathcal{F}_{elast}+\mathcal{F}_{elect}$, is obtained. The stationary orientational configuration $\theta(x)$ is determined by minimizing the free energy. This minimization leads to the Euler-Lagrange equation [8] in the bulk:

$$x^2\frac{d^2\theta}{dx^2}(\cos^2\theta+\kappa\sin^2\theta)+\frac{1}{2}x^2\left(\frac{d\theta}{dx}\right)^2(\kappa-1)\sin 2\theta + x\frac{d\theta}{dx}(\cos^2\theta+\kappa\sin^2\theta)-\frac{1}{2}(1+q_a x^2)\sin 2\theta = 0, \quad (5)$$

with $\theta(x)$ satisfying the following weak anchoring boundary conditions on the cylinders walls at R_1 and R_2, respectively,

$$\left.\frac{d\theta}{dx}\right|_{x=R_1/R_2} = \left.\frac{\frac{1}{2}\left(\frac{R_2}{R_1}\right)\sigma_1\sin 2\theta}{\cos^2\theta+\kappa\sin^2\theta}\right|_{x=R_1/R_2}, \quad (6)$$

$$\left.\frac{d\theta}{dx}\right|_{x=1} = \left.\frac{\frac{1}{2}\sigma_2\sin 2\theta}{\cos^2\theta+\kappa\sin^2\theta}\right|_{x=1}. \quad (7)$$

The quasiescaped radially configuration is radially dependent and can be obtained by solving Eq. (5) subjected to the conditions given by Eqs. (6) and (7).

In what follows, we will present results for the specific case of 4′-n-pentyl-4-cyanobiphenyl (5CB) liquid crystal. The material parameters used are [5] $T_{IN}-T=10\,^\circ$C with $T_{IN}=35\,^\circ$C, $\kappa=1.316$, $K_1=1.2\times10^{-11}$ N, $W_\theta/K_1=40\ \mu\text{m}^{-1}$, and $K_4/K_1=1$. The latter relation between surface and bulk constants of the nematic turns into the following relation between the surface parameters: $\sigma_1=\frac{R_1}{R_2}\sigma_2$. Hence, in this case the boundary conditions given by Eqs. (6) and (7) take the same form.

Numerical solutions of Eq. (5) were calculated by using the shooting method [17] for different values of $x_0=R_1/R_2$, σ_2, and q_a. The cases with $x_0=0.5$, $\sigma_2=2.0$, and q_a

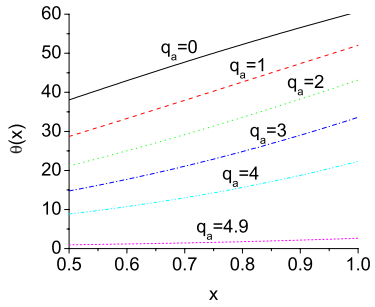

FIG. 2. (Color online) Director configurations θ versus x for 5CB with $x_0=R_1/R_2=0.5$, $\sigma_2=2.0$, and axial electric field parameter $q_a=0,1,2,3,4,4.9$.

$=0,1,2,3,4,4.9$ are depicted in Fig. 2. This plot exhibits that, for $q_a=0$, the values of the orientational angle θ are the largest ones and are determined by both parameters x_0 and σ_2. Notice how the values of θ at the walls diminish by increasing the field until they finally get aligned parallel to z axis for a critical value of the electric field.

Figures 3(a) and 3(b) show the threshold field surface and their corresponding equifield curves plotted as contour lines, respectively, versus the parameters x_0 and σ_2. Here, the threshold field is defined as the critical value of the axially applied electric field necessary to align the director in the z axis. This phase transition has been previously studied [13] and shown that for fields smaller than the critical field, radially dependent configurations take place.

Notice how for $\sigma_2=0$ and $x_0<0.2$ a nonvanishing field is required to align axially the nematic; however, beyond $x_0=0.2$ the nematic liquid crystal is completely aligned only by the influence of the elastic forces. It is worthwhile to mention that for small x_0 values the configurations approach the escaped radial which has a large negative elastic bulk energy. Thus, for small values of $\sigma_2<3.5$ the surface energy corresponding to the inner cylinder reinforces the bulk energy and overpasses that of the outer one, so the resulting elastic force contributes to reduce the q_a value. As should be expected, the effect of the surface forces is stronger when the interior cylinder radius enlarges, so q_a diminishes by increasing x_0. Complimentarily, for larger values of $\sigma_2>3.5$ and $x_0<0.35$ the surface force of the outer cylinder is larger than that of the inner, so the total surface force opposes the electric force. Hence q_a augments by increasing x_0 until it reaches a maximum and then decreases. This change of behavior occurs because when the distance between both cylinder reduces ($x_0>0.35$) the axial configuration is more favored to fill up the space between the cylinders. We should remark that this is a system in small cavities for which the surface anchoring plays an important role in determining the equilibrium configuration of the liquid crystal as that found in Ref. [5].

In Fig. 3(b) we have traced dotted lines to distinguish three regions with different behaviors. For region I, q_a grows monotonically against both x_0 and σ_2. For region II q_a decreases as x_0 increases by keeping σ_2 fixed. Region III q_a grows when σ_2 increases and x_0 remains fixed, until it reaches a maximum to decrease after this. As we discussed above, this changing behavior is the result of the competition between the surface elastic forces in both walls, the elastic bulk force, and the electric field.

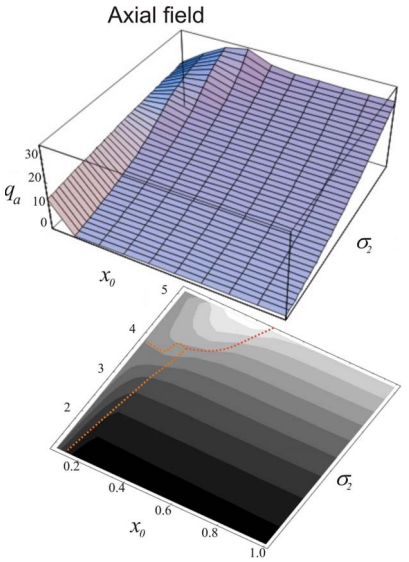

FIG. 3. (Color online) (a) q_a against x_0 and σ_2 for 5CB. (b) Equifield curves are represented by contour lines. Dotted lines separate three regions of different behavior.

B. Radial electric field

Now we shall consider the case of an applied electric field $\mathbf{E}$ acting along the radial direction from the inner cylindrical surface to the outer. In this case the electric free energy is given by

$$F_{elect}=-\frac{1}{2}\int_V \epsilon_{rr}(r)E^2\,dv, \tag{8}$$

where $\epsilon_{rr}(r)$ is an element of the dielectric tensor. We have employed the electrostatic field $\mathbf{E}\equiv-\mathbf{e}_r\Delta\phi/r\ln(R_2/R_1)$ generated between the two coaxial cylinders subjected to a potential difference $\Delta\phi$. Using Eq. (8) and ϵ_{ij}, the electric energy per unit length, $\mathcal{F}_{elect}$, becomes

$$\mathcal{F}_{elect}=-\pi K_1 q_r\int_{R_1/R_2}^{1}\left(\frac{\epsilon_\perp^s}{\epsilon_a^s}+\sin^2\theta\right)\frac{dx}{x}, \tag{9}$$

where the dimensionless parameter q_r is defined as $q_r\equiv\epsilon_a^s\Delta\phi^2/[K_1\ln^2(R_2/R_1)]$. Using Eqs. (2) and (9), the total free energy per unit length, $\mathcal{F}$, is obtained. The stationary orientational configuration $\theta(x)$ is determined by minimizing this free energy. This minimization leads to the Euler-Lagrange equation in the bulk:

$$x^2\frac{d^2\theta}{dx^2}(\cos^2\theta+\kappa\sin^2\theta)+\frac{1}{2}x^2\left(\frac{d\theta}{dx}\right)^2(\kappa-1)\sin 2\theta$$
$$+x\frac{d\theta}{dx}(\cos^2\theta+\kappa\sin^2\theta)+\frac{1}{2}(q_r-1)\sin 2\theta=0, \tag{10}$$

where $\theta(x)$ satisfies the weak anchoring boundary conditions on the cylinders walls at R_1 and R_2, given, respectively, by Eqs. (6) and (7).

Numerical solutions of Eq. (10) were calculated by using the same material parameters as those used for the axial electric field for different values of $x_0=R_1/R_2$, σ_2, and q_r. The cases for $x_0=0.5$, $\sigma_2=2.0$, and $q_r=0,0.2,0.4,0.6,0.8,1.0$ are shown in Fig. 4. This plot clearly shows that, for $q_r=0$, the values of the orientational angle θ are the lowest ones which

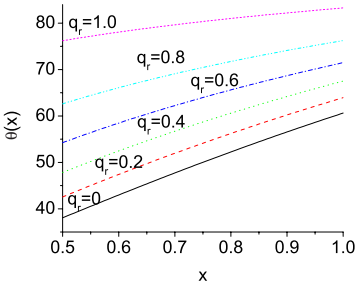

FIG. 4. (Color online) Director configurations θ versus x for 5CB with $x_0=R_1/R_2=0.5$, $\sigma_2=2.0$, and radial electric field parameter $q_r=0,0.2,0.4,0.6,0.8,1.0$.

are determined only by the ratio x_0 and the interaction of the nematic with the walls. Notice how the values of θ at the walls grow up by increasing the field until they finally get radially aligned for a critical value of the electric field.

Figures 5(a) and 5(b) show threshold field surface and equifield curves, respectively, versus x_0 and σ_2. The radial threshold field is defined similarly as in the axial case.

This is also a configurational transition since for values smaller that this critical value the nematic acquires radially dependent textures. In Fig. 3(b) equifield curves are represented as contour lines to show that the threshold fields are essentially hyperbolalike curves, which implies that q_r increases by enlarging either x_0 or σ_2. In contrast to the axial case discussed in last section, here the dependence on both parameters is completely monotonous. This is so because the spatial dependence of the radial electric field $(1/r)$ compensates the effect of the line defect resulting from the escaped radial configuration, obtained in the limit case when $x_0 \to 0$. Another way to stress the difference between both configuration is by noting that Eq. (10) is invariant after a change of scale $r'=ar$, whereas Eq. (5) is not. Hence, the former equation should have a monotonous dependence on x_0.

III. CONCLUDING REMARKS

We have calculated the configurations of a nematic liquid crystal confined between two coaxial cylinders submitted to a low-frequency electric field for arbitrary anchoring boundary conditions for certain realistic values of the elastic parameters.

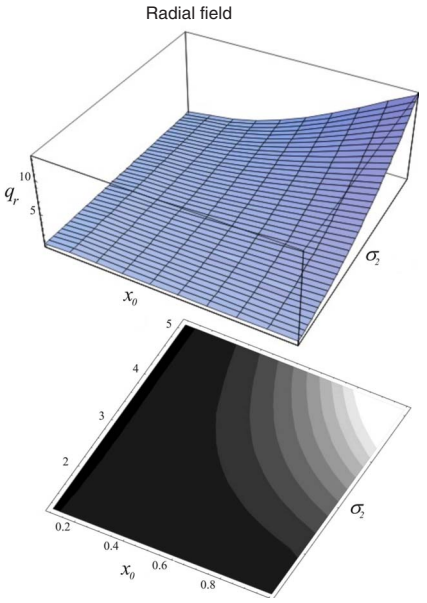

FIG. 5. (Color online) (a) q_r versus x_0 and σ_2 for 5CB. (b) Equifield curves are represented as contour lines.

We demonstrate that to axially orient a nematic liquid crystal confined between two cylinders there exist three regions in the σ_2-x_0 space showing different behaviors, which are essentially the result of the competition between the surface elastic forces at both cylinders and the electric force. In contrast, the behavior of the system under the action of a radial field is quite monotonous because its inversely proportional dependence compensate the augment of elastic bulk energy around the inner cylinder, as its radius decreases.

Our results suggest to use this coaxial nematic cored fiber to design a device for electrically switch the propagation of a desired number of TM modes of optical fields.

We acknowledge the partial support of the Programa Interinstitucional de Colaboración UNISON-UNAM and CONACYT (Estancias de Consolidación 060223) and Grant No. IN117606-3 from DGAPA-PAPITT.

[1] I. E. Dzyaloshinskiĭ, Zh. Eksp. Teor. Fiz. **58**, 1443 (1970) [Sov. Phys. JETP **31**, 773 (1970).
[2] P. E. Cladis and M. Kleman, J. Phys. (Paris) **33**, 591 (1972).
[3] L. D. Landau and E. M. Lifshitz, *Theory of Elasticity* (Pergamon Press, Oxford, 1986).
[4] D. W. Allender, G. P. Crawford, and J. W. Doane, Phys. Rev. Lett. **67**, 1442 (1991).
[5] G. P. Crawford, D. W. Allender, and J. W. Doane, Phys. Rev. A **45**, 8693 (1992).
[6] S. Kralj and S. Zumer, Phys. Rev. E **51**, 366 (1995).
[7] S. V. Burylov, Zh. Eksp. Teor. Fiz. **112**, 1603 (1997) [J. Exp. Theor. Phys. **85**, 873 (1997).
[8] A. Corella-Madueño and J. Adrián Reyes, Opt. Commun. **264**, 148 (2006).
[9] J. W. Doane *et al.*, Mol. Cryst. Liq. Cryst. **165**, 51 (1988).
[10] G. Srajer, F. Lonberg, and R. B. Meyer, Phys. Rev. Lett. **67**, 1102 (1991).
[11] O. D. Lavrentovich, Phys. Scr. **T39**, 394 (1991).
[12] A. Saupe, J. Chem. Phys. **75**, 5118 (1981).
[13] P. Halevi, J. A. Reyes-Avendaño, and J. A. Reyes-Cervantes, Phys. Rev. E **73**, 040701(R) (2006).
[14] T. T. Larsen, A. Bjarklev, D. S. Hermann, and J. Broeng, Opt. Express **11**, 2589 (2003).
[15] M. Petrov *et al.*, J. Optoelectron. Adv. Mater. **9**, 446 (2007).
[16] A. Rapini and M. Papoular, J. Phys. (Paris), Colloq. **30**, C4–54 (1969).
[17] W. H. Press, B. P. Flannery, S. A. Teukolsky, and W. T. Vetterling, *Numerical Recipes: The Art of Scientific Computing* (Cambridge University Press, Cambridge, England, 1986).